# A new approach for studying nucleation phenomena using molecular simulations: Application to $CO_2$ hydrate clathrates

Ravi Radhakrishnan and Bernhardt L. Trout[a)]
*Massachusetts Institute of Technology, Cambridge, Massachusetts 02139*

(Received 13 February 2002; accepted 23 April 2002)

We use an order-parameter formulation, in conjunction with non-Boltzmann sampling to study the nucleation of clathrate hydrates from water–$CO_2$ mixtures, using computer simulations. A set of order parameters are defined: $\Phi_i^{gg}$ ($i=1,2,...,n$ and gg for guest–guest), which characterize the spatial and orientational order of the $CO_2$ molecules, and $\Phi_i^{hh}$ (hh for host–host), which govern the ordering of the water molecules. These are bond-orientational order parameters based on the average geometrical distribution of nearest-neighbor bonds. The free-energy hypersurface as a function of the order parameters is calculated using the Landau–Ginzburg approach. The critical cluster size that leads to the nucleation of the clathrate phase is determined accurately by analyzing the free energy surface. We find that the nucleation proceeds via ''the local structuring mechanism,'' i.e., a thermal fluctuation causing the local ordering of $CO_2$ molecules leads to the nucleation of the clathrate, and not by the current conceptual picture, called ''the labile cluster hypothesis.'' The local ordering of the guest molecules induces ordering of the host molecules at the nearest- and next-to-nearest-neighbor shells, which are captured by a three-body host–host order parameter, $\zeta^{hh}$; these thermodynamic fluctuations lead to the formation of the critical nucleus. Our results are significant in understanding the proposed sequestration of $CO_2$ by direct ocean injection in order to mitigate the greenhouse effect. © *2002 American Institute of Physics.* [DOI: 10.1063/1.1485962]

## I. INTRODUCTION

The viability of ocean storage as a greenhouse gas mitigation option is a topic of ongoing research and debate.[1] The ocean represents a large potential sink for anthropogenic $CO_2$ emitted into the atmosphere, and in fact, it has been predicted that eventually over 80% of anthropogenic $CO_2$ will end up in the ocean at equilibrium.[2] There have been several methods proposed for injecting $CO_2$ into the ocean. A leading candidate is to transport the $CO_2$ in a pipe to moderate ocean depths (from 1000 to 2000 m), where upon release as liquid droplets it will form a plume and dissolve[3] into the ocean. In this case, there is formation of clathrate hydrate of structure I (a crystalline solid that includes $CO_2$ molecules in cages formed by water molecules, see e.g., Sloan[4]), at the interface of $CO_2$ and sea water, that impacts the rate of dissolution of $CO_2$ in the ocean in addition to the hydrodynamics of the clathrate–hydrate coated droplets. In order to characterize the process of injection and dissolution of liquid $CO_2$, two required physical properties are the rate of diffusion of $CO_2$ in the clathrate hydrate phase and the rate of nucleation of $CO_2$ hydrate. Recently, we reported a theoretical study[5,6] using molecular simulations, in which a mechanism for the diffusion of $CO_2$ molecules in the hydrate phase was proposed, the diffusivity of $CO_2$ in the hydrate was computed, and a consistent and verifiable macroscopic model for the dissolution of hydrate–clathrate coated droplets of liquid $CO_2$ was proposed. In this paper, we focus on the nucleation of $CO_2$ hydrates. Moreover, we present a general approach for studying nucleation and order–disorder transitions.

Equilibrium properties of the $CO_2$/sea-water system have been well researched from an experimental standpoint.[7–11] In particular, the clathrate hydrate forming conditions ($T<285$ K and $P>4$ MPa) are well established. For a complete phase diagram see, e.g., Wendland *et al.*[9] Several experiments have been performed under conditions mimicking the direct injection process and have attempted to study the dissolution rate of $CO_2$ in sea water.[12–24] Under direct injection conditions, the injected $CO_2$ is in the form of a liquid droplet and a thin spherical shell of $CO_2$ clathrate hydrate of structure I is observed to form around the $CO_2$ drop, separating it from the sea water. The process of hydrate formation has many similarities with that of crystallization, i.e., it can be divided into a nucleation phase and a growth phase. For $CO_2$ clathrates, the nucleation phase involves the formation of a hydrate nucleus of a critical size at the liquid–liquid interface of $CO_2$ and water. This homogeneous nucleation process is believed to be stochastic in nature, i.e., the critical nucleus is formed because of a local thermodynamic fluctuation in the system. The formation of the critical nucleus is followed by the spontaneous growth of the hydrate phase at the interface. In the past, researchers have described the nucleation process using classical nucleation theory,[25–27] according to which the free energy of the formation of the nucleus is calculated assuming that the formed nucleus has bulk-like properties. The size of the critical nucleus, $r_c$, is one that maximizes the sum of the surface excess free energy due to the interface between the bulk and the nucleus and the

a)Author to whom all correspondence should be addressed; electronic mail: trout@mit.edu

 

volume excess free energy of the nucleus relative to the bulk phase and is given by

$$r_c = \frac{2\gamma}{\Delta g}. \quad (1)$$

In Eq. (1), $\gamma$ is the surface free energy density associated with the crystalline–liquid interface and $\Delta g$ is the difference in free energies per unit volume of the crystalline and liquid phases at the given temperature. If the size of the nucleus exceeds $r_c$, the system can spontaneously lower its free energy through the growth of the crystal-like nucleus. Larson and Garside[53] calculated the size of the critical nucleus for methane clathrate hydrates to be ≈32 Å, at a supercooling of 5 K. Bishnoi and co-workers[28] have taken a unified approach to describe nucleation and growth in which the nucleation is described according to classical nucleation theory and the growth phase is modeled as a chemical reaction. The authors suggested that the rate constants that describe the growth of the hydrate phase be obtained by fitting the reaction model to experimental data on the uptake of the guest molecules versus time.[29,30] The classical nucleation approach is faced with two shortcomings: (1) the macroscopic treatment of the nucleus, which is of a linear dimension of a few nanometers, leads to substantial errors in the excess free energy;[31] (2) the pathway by which the nucleus forms and the exact structure of the hydrate nucleus remain unknown. In light of addressing the latter point Sloan and co-workers have proposed the labile cluster hypothesis as a possible mechanism for the formation of the critical nucleus.[4,32,33] Based on the available experimental evidence[4,32] and molecular simulation results,[34] the researchers proposed that the hydrate formation is initiated by the following three steps: (1) labile clusters are spontaneously formed when a hydrophobic solute is dissolved in water under hydrate forming conditions; (2) the labile clusters (consisting of a solute molecule surrounded by 20–24 water molecules in the first coordination shell) associate with each other to assemble the hydrate nucleus; (3) the association occurs in different configurations of which only a few will lead to the correct hydrate structure. Based on this hypothesis, Sloan and Fleyfel modeled the nucleation process as a set of chemical reactions that describe steps (1)–(3). The rate constants were fitted to hydrate kinetic data on the uptake of solute molecules versus time, therefore the model was not predictive. Moreover, the molecular basis for the above-mentioned hypothesis was not established. Kvamme[35] proposed a variation of the labile cluster hypothesis, that the assembly of the labile clusters takes place at the vapor–liquid interface rather than in the bulk liquid. However a quantitative estimation of the rate of nucleation was not attempted.

In this paper, we propose a rigorous methodology for computing the reversible work for embryo formation within the framework of classical statistical mechanics and making use of molecular simulations. Using our free energy formalism, we evaluate the validity of the labile cluster hypothesis, and provide a molecular basis for the hydrate nucleation process. We estimate the rate of nucleation by calculating the free energy barrier for the formation of the critical nucleus and using transition state theory. The formalism that we describe is generally applicable in the study of (a) equilibrium properties associated with any order–disorder phase transition, (b) mechanism of nucleation of the ordered phase in the supercooled state.

## II. METHODOLOGY

We perform Monte Carlo simulations in the isothermal, isobaric ensemble (fixing the number of molecules, $N$, the pressure, $P$, and the temperature, $T$, of the $CO_2$–$H_2O$ binary system). The intermolecular potential for water is modeled using the TIP4P potential[36] and that for $CO_2$ is modeled using the Harris and Yung potential.[37] All the bond lengths and the bond angles of the individual molecules were kept fixed during the Monte Carlo simulations. The calculated thermophysical data of the pure phases and solubility data for the binary system, using the respective models, are in very close agreement with the experimental measurements,[36–38] making these models a suitable choice for aqueous phase simulations. We chose an initial system size of a 48 Å cubical box for the free energy calculations, and a rectilinear box of 192 Å×24 Å×24 Å for calculating the properties of liquid $CO_2$–liquid $H_2O$ interface. The temperature and pressure in the simulations were maintained at 220 K and 4 MPa, respectively. The TIP4P model water has a freezing temperature of about 250 K ±30 K,[39–41] thus the chosen temperature and pressure conditions of our model system are expected to be within the phase boundary of the $CO_2$ clathrate,[9] which in the real system, correspond to 273 K and 4 MPa. Under these conditions the number of $H_2O$ and $CO_2$ molecules in the 48 Å box are 2944 and 496, respectively. Periodic boundary conditions were applied in all three directions and the method of Ewald summation was used to account for the long-range electrostatic interactions due to the partial charges of water and $CO_2$. Typical production runs involved averaging the properties over a billion MC configurations. A parallel version of the Monte Carlo program was used to run on 8–16 processors.

The key to a successful theory that describes the process of nucleation is the determination of a set of dynamical variables (order parameters and their conjugate fields) that govern the phase transition, and a rigorous formalism to compute the reversible work for the ''embryo formation.'' The order parameters are system dependent (i.e., depend on the particular order–disorder transition of interest), and are usually determined based on the symmetry of the ordered phase and how it differs from the disordered phase, while the reversible work for embryo formation (formation of the critical nucleus) is defined using thermodynamics and statistical mechanics.

### A. Order parameters

We choose a set of scalar order parameters based on the distribution of nearest-neighbor bonds (bond-orientational order parameters), that are sensitive to the periodic density modulations in the crystal phase. The bond-orientational order parameters are scalar functions that are used to expand the local density $\rho(\mathbf{r})$ in terms of spatial and orientational basis functions.[42] Since the free energy is a unique functional of $\rho(\mathbf{r})$, including the relevant functions that constitute $\rho(\mathbf{r})$,

ensures a successful theory. However, recognizing that the local density at position $\mathbf{r}$ is coupled to that at position $\mathbf{r}'$ by the direct correlation function, Ramakrishnan and Youssouf[43] demonstrated that choosing a finite number of scalar functions that represent the pair correlation function $g(\mathbf{r})$ at the nearest-neighbor and next-neighbor-level, together with an exact treatment of the direct correlation function, is sufficient to characterize the free energy surface.

Since the set of scalar order parameters have to be invariant under global translation or rotation of the coordinate system (the crystal axes may be oriented in any direction with respect to our coordinate frame of reference), we use the three-dimensional bond orientational order parameters introduced by Steinhardt *et al.*[44] to characterize the ordering of the water molecules and the $CO_2$ molecules in the clathrate phase. These order parameters are defined as follows: each nearest-neighbor bond has a particular orientation in space with respect to a reference axis, which can be described by the spherical coordinates $(\theta,\phi)$. Nearest neighbors were identified as those molecules that were less than a cutoff distance $r_{\mathrm{nn}}$ away from a given molecule. One can then define the global order parameter $\bar{Q}_{lm}$,

$$\bar{Q}_{lm} \equiv \frac{1}{N_b} \sum_{i=1}^{N_b} Y_{lm}(\theta_i, \phi_i), \tag{2}$$

where the index $i$ runs over the total number of nearest-neighbor bonds $N_b$ and the $Y_{lm}$'s denote the spherical harmonics. In view of the fact that the order parameter does not depend on the overall orientation of the crystal in the simulation cell, rotationally isotropic combinations of the $\bar{Q}_{lm}$'s are defined as

$$Q_l \equiv \left( \frac{4\pi}{2l+1} \sum_{m=-l}^{+l} |\bar{Q}_{lm}|^2 \right)^{1/2} \tag{3}$$

and

$$W_l = \frac{1}{(\Sigma_m |\bar{Q}_{lm}|^2)^{3/2}} \sum_{m_1,m_2} \begin{pmatrix} l & l & l \\ m_1 & m_2 & -m_1-m_2 \end{pmatrix} \times \bar{Q}_{lm_1} \bar{Q}_{lm_2} \bar{Q}_{l(-m_1-m_2)}. \tag{4}$$

The matrix in Eq. (4) is a representation of the Wigner 3J symbols (see, e.g., Landau[45]). We define $Q_l^{\mathrm{gg}}$, $W_l^{\mathrm{gg}}$ associated with the guest–guest ordering, and $Q_l^{\mathrm{hh}}$, $W_l^{\mathrm{hh}}$ associated with the host–host ordering. Our choice of the cutoff distance $r_{\mathrm{nn}}$ to define the nearest-neighbor bonds are based on the radial distribution functions, $g_{\mathrm{hh}}(r)$ and $g_{\mathrm{gg}}(r)$. The $g_{\mathrm{hh}}(r)$ function is defined with respect to the oxygen–oxygen distance between two water molecules, and the $g_{\mathrm{gg}}(r)$ function is defined with respect to the carbon–carbon distance between two $CO_2$ molecules (see Fig. 1). Thus for host–host order parameters, the cutoff $r_n^{\mathrm{hh}}$ was chosen to be close to the value at which the first peak in $g_{\mathrm{hh}}(r)$ ends [the first peak of $g(r)$ defines the first coordination shell]. Similarly, the cutoff for the guest–guest order parameters were chosen to count the neighboring guest molecules in the first coordination shell. From the $g_{\mathrm{gg}}(r)$ function for the clathrate phase in Fig. 1, it is clear that two such values are needed, as the $g_{\mathrm{gg}}(r)$ function remains zero in the clathrate phase (unlike the liquid phase) for distances much larger than the $\sigma_{\mathrm{gg}}$, the effective Lennard-Jones diameter for $CO_2$. A slight tuning of the cutoff distances were necessary in order to avoid counting of some next-to-nearest-neighbor molecules, due to local fluctuations in the ordered phase (the guest molecules in the clathrate phase do not always occupy the center of the cages). The criterion for the choice of the cutoffs is that which maximizes the difference in the values of the order parameters between the disordered and the ordered phase. The typical values of the Steinhardt order parameters ($Q_l$'s and $W_l$'s) for the liquid and clathrate phase are given in Table I.

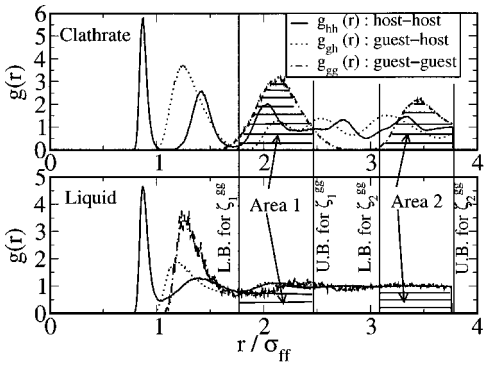


FIG. 1. The host–host, guest–host, and guest–guest radial distribution functions, $[g_{\mathrm{hh}}(r), g_{\mathrm{gh}}(r), g_{\mathrm{gg}}(r)]$, in the clathrate phase and the liquid phase at equilibrium ($CO_2$ mole fraction, $X_{CO_2} = 0.14$), at 220 K and 4 MPa. The distances are scaled by $\sigma_{ff} = 3.154$ Å, which is the Lennard-Jones diameter of TIP4P water. "LB" and "UB" are lower and upper bounds in the definition of the $\zeta_1^{\mathrm{gg}}$ and $\zeta_2^{\mathrm{gg}}$ order parameters. These were tuned as described in Sec. II A.

For water molecules, we employ the tetrahedral order parameter, which measures the degree to which the nearest-neighbor water molecules are tetrahedrally coordinated with respect to a given water molecule.[46,47] The tetrahedral order parameter, $\zeta^{\mathrm{hh}}$, is defined as follows:

$$\zeta^{\mathrm{hh}} = \frac{1}{N} \sum_{N} \left[ 1 - \frac{3}{8} \sum_{i=1}^{3} \sum_{j=i+1}^{4} (\cos \psi_{ij} + 1/3)^2 \right], \tag{5}$$

TABLE I. Order parameters in clathrate and liquid.

| Order parameter | Clathrate structure I | Liquid |
|---|---|---|
| Guest–guest | | |
| $Q_4^{\mathrm{gg}}$ | 0.0 | 0.0 |
| $Q_6^{\mathrm{gg}}$ | 0.0 | 0.0 |
| $W_4^{\mathrm{gg}}$ | 0.15 | 0.0 |
| $W_6^{\mathrm{gg}}$ | 0.0 | 0.0 |
| $\zeta_1^{\mathrm{gg}}$ | 1.0 | 0.43 |
| $\zeta_2^{\mathrm{gg}}$ | 1.0 | 0.67 |
| Host–host | | |
| $Q_4^{\mathrm{hh}}$ | 0.0 | 0.0 |
| $Q_6^{\mathrm{hh}}$ | 0.0 | 0.0 |
| $W_4^{\mathrm{hh}}$ | −0.15 | 0.0 |
| $W_6^{\mathrm{hh}}$ | 0.0 | 0.0 |
| $\zeta^{\mathrm{hh}}$ | 1.0 | 0.63 |

where $N$ is the number of water molecules, the indices $i,j$ run over the four nearest neighbors of a given water molecule, and $\psi_{ij}$ is the angle between the nearest-neighbor bond associated with molecule $i$ and that of molecule $j$. Therefore, $\zeta^{\mathrm{hh}}$ is a three-body order parameter which ensures local tetrahedral symmetry around each water molecule. The typical values of the tetrahedral order parameter ($\zeta^{\mathrm{hh}}$) for the liquid and clathrate phase are given in Table I.

The tetrahedral order-parameter defines the ordering of the water molecules in the clathrate satisfactorily; however, to describe the ordering of the guest molecules, the Steinhardt order parameters alone are not sufficient. The reason being that there is enough freedom for the guest molecules within each cage such that the translation of the guest molecules within the cage destroys the orientational symmetry of the guest–guest nearest-neighbor bonds. Nevertheless, the translational symmetry is broken for the arrangement of the guest molecules in the clathrate phase. This fact is drawn out clearly in the radial distribution functions (see Fig. 1): $g_{\mathrm{gg}}(r)$ associated with the clathrate phase shows clearly defined peaks, and troughs that pass through zero. We therefore define the order parameter, $\zeta_1^{\mathrm{gg}}$ as the ratio of the areas under the $g_{\mathrm{gg}}(r)$ functions (between the bounds of the first peak in the clathrate phase, see Fig. 1), of the current configuration to that in the clathrate phase,

$$\zeta_1^{\mathrm{gg}}=\frac{\text{area 1 in the current configuration}}{\text{area 1 in clathrate}}, \tag{6}$$

where, ''area 1'' is defined in Fig. 1. Similarly, $\zeta_2^{\mathrm{gg}}$ is defined with respect to the second peak in $g_{\mathrm{gg}}(r)$ of the clathrate phase. The typical values of the guest–guest order parameters ($\zeta_i^{\mathrm{gg}}$) for the liquid and clathrate phase are given in Table I. By definition, the values of $\zeta_i^{\mathrm{gg}}$ are close to unity in the clathrate phase and significantly less than one in the liquid phase. To summarize, the ordering along the $\zeta_i^{\mathrm{gg}}$ coordinates affects the dispersion of $CO_2$ molecules, which otherwise tend to agglomerate due to hydrophobic interactions. Ordering along the $W_4^{\mathrm{gg}}$ coordinate restores the rotational symmetry that exists in the clathrate, and the ordering along the $\zeta^{\mathrm{hh}}$ ensures that the water molecules are perfectly tetrahedrally coordinated, as in the clathrate. Therefore, we propose that the guest–guest Steinhardt order parameter, $W_4^{\mathrm{gg}}$, tetrahedral order parameter, $\zeta^{\mathrm{hh}}$, and the guest–guest order parameters ($\zeta_1^{\mathrm{gg}},\zeta_2^{\mathrm{gg}}$) based on $g_{\mathrm{gg}}(r)$, are sufficient to describe the symmetry of the clathrate phase. This will be validated *a postieri*.

### B. Landau free energy method

In order to calculate the free energy, we use the Landau–Ginzburg (LG) formalism[50] in conjunction with the order parameters, $\Phi_i$, $i=1,...,4$ (where $\Phi_1=\zeta_1^{\mathrm{gg}}$, $\Phi_2=\zeta_2^{\mathrm{gg}}$, $\Phi_3=W_4^{\mathrm{gg}}$, and $\Phi_4=\zeta^{\mathrm{hh}}$). For the general case of a spatially varying order parameters $\Phi_i(\mathbf{r})$, $i=1,...,4$, the probability distribution function of the order parameters $P[\tilde{\Phi}_1(\mathbf{r}),\tilde{\Phi}_2(\mathbf{r}),\ldots]$ is defined as

$$P[\tilde{\Phi}_1(\mathbf{r}),\tilde{\Phi}_2(\mathbf{r}),\ldots]=\frac{1}{Q_{NPT}}\int dV\int d\tau_{\mathrm{rot}}^N\Pi_i\left\{\int D_N[\Phi_i(\mathbf{r})]\right\}\frac{1}{N!\lambda^{3N}}\times\Pi_i\{\delta(\tilde{\Phi}_i(\mathbf{r})-\Phi_i(\mathbf{r}))\}\exp(-\beta H_N-\beta PV) \tag{7}$$

$Q_{NPT}$ is the partition function in the isothermal-isobaric ensemble, $V$ is the volume of the system, $\beta=1/k_BT$, $\lambda$ is the de Broglie wavelength, and $H_N$ is the configurational Hamiltonian of the system. The path integral notation $D_N[\Phi_i(\mathbf{r})]$ should be interpreted as[42]

$$\Pi_i\left\{\int D_N[\Phi_i(\mathbf{r})]\right\}\equiv\Pi_i\left\{\lim_{v_0\to 0}\Pi_\alpha\int d\Phi_{i,\alpha}\right\}=\int_{\mathbf{r}^N}d\mathbf{r}^N. \tag{8}$$

Equation (8) defines the path integral in terms of a trace over a discrete number of sites $\alpha$, and $v_0$ represents the volume per site. The coordinates of the center of mass of the molecules are represented by $\mathbf{r}^N$, and $\tau_{\mathrm{rot}}^N$ are the Euler angles representing the rotational degrees of freedom of each of the molecules about their center of mass. The Landau free energy $\Lambda[\tilde{\Phi}_1(\mathbf{r}),\tilde{\Phi}_2(\mathbf{r}),\ldots]$ is defined as

$$\exp(-\beta\Lambda[\tilde{\Phi}_1(\mathbf{r}),\tilde{\Phi}_2(\mathbf{r}),\ldots])=\int dV\int d\tau_{\mathrm{rot}}^N\Pi_i\left\{\int D_N[\Phi_i(\mathbf{r})]\right\}\frac{1}{N!\lambda^{3N}}\times\Pi_i\{\delta(\tilde{\Phi}(\mathbf{r})-\Phi(\mathbf{r}))\}\exp(-\beta H_N-\beta PV), \tag{9}$$

$$\Lambda[\Phi_1(\mathbf{r}),\Phi_2(\mathbf{r}),\ldots]=-k_BT\ln(P[\Phi_1(\mathbf{r}),\Phi_2(\mathbf{r}),\ldots])+\text{constant}. \tag{10}$$

Equation (10) follows from Eq. (9). The Gibbs free energy, $G=-k_BT\ln(Q_{NPT})$, is then related to the Landau free energy by the path integral,

$$\exp(-\beta G)=\Pi_i\left\{\int D_N[\Phi_i(\mathbf{r})]\right\}\times\exp(-\beta\Lambda[\Phi_1(\mathbf{r}),\Phi_2(\mathbf{r}),\ldots]). \tag{11}$$

To calculate the Gibbs free energy of a particular phase $A$, the limits of integration in Eq. (11) are from the minimum value of $\Phi$ to the maximum value of $\Phi$, that characterizes phase $A$.

### C. Implementation of the LG formalism

The probability distribution function $P[\Phi_1(\mathbf{r}),\Phi_2(\mathbf{r}),\ldots]$ is calculated during a simulation run by collecting statistics of the number of occurrences of particular values of $\Phi_1(\mathbf{r})$, $\Phi_2(\mathbf{r}),\ldots$ during the course of the $NPT$ simulations. This is accomplished by constructing a multidimensional histogram with respect to $\Phi_1(\mathbf{r})$, $\Phi_2(\mathbf{r}),\ldots$ values. In the absence of a spatially varying external potential, the equilibrium phases are homogeneous, therefore only two cases of the inhomogeneous order parameters need to be considered: the first is the global order parameter which is the spatial average of the inhomogeneous order parameter over the entire volume, $\Phi_i^{\mathrm{global}}$. The second is a cluster order parameter, $\Phi_i^{\mathrm{cluster}}$, defined as the spatial average of the order parameter

is a small region of space that is a subset of the total volume. Since nucleation occurs via the formation of a critical nucleus, the cluster order parameters are sufficient to describe the nucleation process, and one does not have to deal with the generic $\Phi_i(\mathbf{r})$. The precise definition of the cluster order parameters is given in Sec. III. It turns out that reliable statistics for up to a four-dimensional probability distribution function of the global and cluster order parameters can be collected in conjunction with umbrella sampling as described in the following.[48–51]

As will become clear from the discussion on liquid–liquid interface (Sec. III A), the hydrophobic effect drives the liquid–liquid phase separation of $CO_2$ and $H_2O$ mixture that leads to the agglomeration of the $CO_2$ molecules. In the clathrate phase, however, the $CO_2$ molecules are uniformly dispersed and are separated by a shell of water molecules. Therefore, it is reasonable to expect that the least probable of the thermodynamic fluctuations is one that favors ordering along the $\zeta_1^{\mathrm{gg,cluster}}$ coordinate. To calculate $P[\Phi_1,\ldots,\Phi_4]$, (here $\Phi_i$ can either be a global or a cluster order parameter), one order parameter coordinate, $\Phi_1=\zeta_1^{\mathrm{gg,cluster}}$, is chosen to be the principal coordinate, and divided into thirty windows. As a first estimate, a probability distribution, $P_1[\Phi_1,\ldots,\Phi_4]$, is calculated separately in each of the windows, by collecting statistics in the form of a four-dimensional histogram in $\Phi_i$, $i=1,\ldots,4$. We start with a well equilibrated liquid phase, and perform normal $NPT$ simulations. During the course of the simulation we record the minimum and maximum values of $\Phi_i$ and $P[\Phi_1,\ldots,\Phi_4]$ in that range of $\Phi_i$. This defines our first window of $\Phi_1$. Starting with the configuration corresponding to maximum value of $\Phi_1$ from the first window, we perform $NPT$ simulations in the second window. We constrain the order parameter $\Phi_1$ to be within the range of the second window (the lower bound of $\Phi_1$ for the second window is slightly less than the upper bound of $\Phi_1$ in the first window and so on). This process is continued until we span the complete range of the order parameter, $\Phi_1$. During this process the other three order parameters are not constrained, but instead left to evolve ergodically as the system explores the phase space. The individual pieces of the Landau free-energy hypersurface from each window are calculated using Eq. (10). Since the pieces are determined only to an arbitrary constant, the constant term is adjusted in each window to make the free energy surface continuous along the coordinate $\Phi_1$. This procedure is done as follows: The first-order distribution function, $\Lambda^{(1)}[\Phi_1]$, is calculated by integrating $\Lambda[\Phi_1,\ldots,\Phi_4]$ with respect to all order parameters except $\Phi_1$. Suitable constants are added to $\Lambda^{(1)}[\Phi_1]$ in each window to make the function continuous (and visibly differentiable) along the coordinate $\Phi_1$. In our scheme, this adjustment ensures the continuity of the Landau free energy hypersurface along all the order-parameter coordinates. Having obtained the first estimate of the Landau free energy hypersurface and $\Lambda^{(1)}[\Phi_1]$ without the use of any weighting function in the umbrella sampling, a successive set of simulations are then performed in each of the windows by using a weighting function $w\{\Phi_1\}=\exp(+\beta\Lambda^{(1)}[\Phi_1])$ in addition to the usual acceptance criteria for the probabilities in the $NPT$ simulations.[48,49,51] This results in a new set of probability distribution functions, $P[\Phi_1,\ldots,\Phi_4]$, and consequently $\Lambda[\Phi_1,\ldots,\Phi_4]$. The procedure for adjusting the constants to make the free energy hypersurface continuous is repeated with the new distribution functions. In theory, the accuracy of the computed free energy surface increases with successive iterations, however in practice it is established that the distribution functions converge just with one iteration.[49] The Gibbs free energy is calculated by performing a numerical integration of Eq. (11). During the free energy simulations, $g(r)$ functions and snapshots are monitored to ensure that the resulting phase is indeed a clathrate phase.

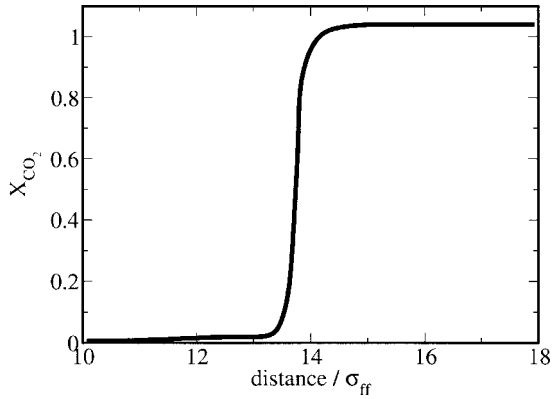


FIG. 2. The equilibrium distribution of the mole fraction of $CO_2$ across the interface. The interface width is of the order of 8 Å.

## III. RESULTS

### A. The $CO_2$–$H_2O$ interface

It is a known experimental fact that the $CO_2$ hydrate nucleates at the liquid–liquid interface of $CO_2$ and $H_2O$.[12–24] Thus, it is important to understand the nature of this interface. The interface was equilibrated by sandwiching a liquid $CO_2$ phase (saturated with water) between two $H_2O$ phases (saturated with $CO_2$). The system size was chosen to be 192 Å×24 Å×24 Å, and comprised of a total of 1336 water molecules and 512 $CO_2$ molecules between the three phases. Energy minimization was performed in the two regions dividing the liquid $CO_2$ phase from the $H_2O$ phases. The system was equilibrated by performing 100 million MC steps. The variation of the mole fraction of $CO_2$ across the interface after equilibration was calculated by averaging over an additional 100 million MC steps and the result is shown in Fig. 2. The distribution of the mole fraction across the interface was calculated by discretising the spatial coordinate perpendicular to the interface, and collecting histograms of the number of $CO_2$ and $H_2O$ molecules along this coordinate. Due to the hydrophobic nature of the $CO_2$ molecules, the interface is sharp, i.e., the variation of the mole fraction across the interface occurs in the range of 8 Å ($1\,\sigma_{ff}=3.154$ Å). It is worthwhile to note that in this length scale, the mole fraction of $CO_2$, $X_{CO_2}$, decreases from $\simeq 1.0$ to 0.013, passing through $X_{CO_2}=0.14$ (the stoichiometric composition of $CO_2$ in a clathrate with all cages occupied).

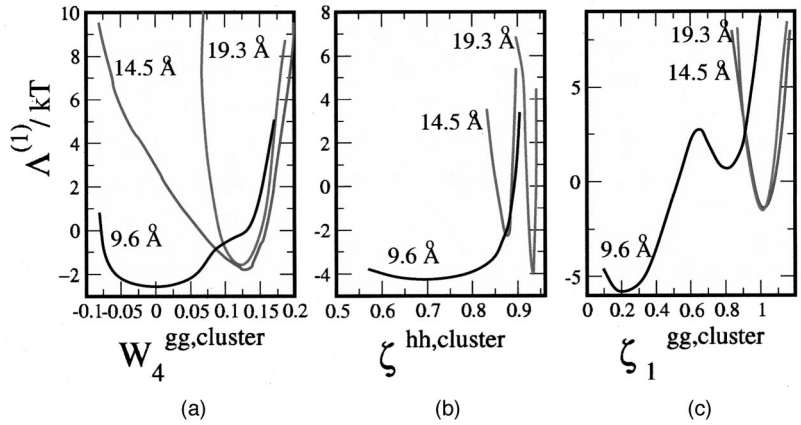


FIG. 3. First-order distribution functions for three different sizes of cluster implants (9.6, 14.5, and 19.3 Å) with respect to (a) $W_4^{gg,cluster}$, (b) $\zeta^{hh,cluster}$, (c) $\zeta_1^{gg,cluster}$.

### B. Hydrate cluster implant and growth

In order to estimate the size of the critical nucleus of the $CO_2$ hydrate that leads to the spontaneous growth of the hydrate phase at the interface, we implanted hydrate clusters of different sizes in a $CO_2$ and $H_2O$ liquid solution (at the stoichiometric mole fraction, $X_{CO_2}=0.14$), and let the system equilibrate. We note that such a high concentration of $CO_2$ is found only near the interface as discussed previously. The interface between the implanted cluster and the liquid mixture was relaxed by energy minimization, prior to performing the Monte Carlo runs. A total of one billion MC steps were performed for each cluster size during which the size of the implanted cluster was monitored. The results for two different sizes of the implanted cluster are described in the following: As the system evolved, the implanted cluster of linear dimension 19.3 Å expanded in size to encompass the whole system, while an implanted cluster of 9.6 Å diminished in size and disintegrated into solution. From these results we conclude that the critical nucleus size for the formation of the $CO_2$ hydrate phase lies in between 9.6 and 19.3 Å. This result is consistent with the estimate of the critical cluster size for methane hydrate previously reported by Báez and Clancy[52] using molecular dynamics methods. In order to obtain a better estimate of the ''critical nucleus size,'' we analyzed the thermodynamic stability of the different cluster implants, by mapping the free energy hypersurface of inhomogeneous system (implanted cluster in a liquid solution) as a function of the cluster order parameters. This procedure is described in the following.

An implanted cluster is viewed as an inhomogeneous phase in which the order parameters are spatially varying. For example, the order parameters $W_4^{gg}(\mathbf{r})$ and $\zeta^{hh}(\mathbf{r})$ take on values close to that in the clathrate phase in the region of the implanted cluster, and liquid-like values outside the region of the implanted cluster. We can then define an order parameter with reference to the cluster (for example, $W_4^{gg,cluster}$) as follows:

$$W_4^{gg,cluster}=\frac{1}{V_{cluster}}\int_{V_{cluster}} d\mathbf{r}\, W_4^{gg}(\mathbf{r}). \tag{12}$$

In Eq. (12), $V_{cluster}$ is the volume occupied by the implanted cluster. Other cluster order parameters ($\zeta^{hh,cluster}$, etc.) are defined similar to Eq. (12). It must be remarked that we do not not assume the shape of the cluster to be spherical. Instead, we identify a specific number of guest molecules being part of the cluster. The cluster order parameters are calculated based on this set of guest molecules and their neighboring host molecules. Therefore, the cluster can take up any arbitrary shape in the simulation box.

The stability of the implanted cluster is determined by calculating the Landau free energy hypersurface as a function of the cluster order parameters, $\Lambda[W_4^{gg,cluster}, \zeta^{hh,cluster},\ldots]$. The global minimum in the Landau free energy hypersurface of a stable cluster (i.e., one that expands in size) occurs at the values of the cluster order parameters close to that of the clathrate phase. On the other hand, the global minimum in the Landau free energy hypersurface of an unstable cluster (i.e., one that disintegrates into solution) occurs at the values of the cluster order parameters close to that of the liquid phase. The first-order distribution functions, $\Lambda^{(1)}[\zeta_1^{gg,cluster}]$, $\Lambda^{(1)}[\zeta^{hh,cluster}]$, and $\Lambda^{(1)}[W_4^{gg,cluster}]$ for the implanted clusters of three different sizes, 9.6, 14.5, and 19.3 Å are shown in Fig. 3. The first-order distribution function of a particular cluster parameter, $\Lambda^{(1)}[W_4^{gg,cluster}]$, is related to the probability of finding the system with a particular value of the cluster order parameter $W_4^{gg,cluster}$, irrespective of the values of the other cluster order parameters ($\zeta^{hh,cluster}$, etc.). Since the first-order distribution function is a projection of the Landau free energy hypersurface on a particular order-parameter coordinate, it is easily visualized in a two-dimensional plot. It is clear from Fig. 3 that the global minimum in the Landau free energy hypersurface for the 9.6 Å cluster implant occurs at values of $W_4^{gg,cluster}=0$, $\zeta^{hh,cluster}=0.6$, and $\zeta_1^{gg,cluster}=0$, which correspond to the order parameter values in the liquid phase, while the global minimum for the 14.5 and 19.3 Å cluster implants occur at values of $W_4^{gg,cluster}=0.14$, $\zeta^{hh,cluster}=0.9$, and $\zeta_1^{gg,cluster}=0.9$, which correspond to order parameter values in the clathrate phase. Therefore we conclude that the size of the critical nucleus (at 220 K, 4 MPa) is between 9.6 and 14.5 Å. The significance of the bounds for the size of the critical nucleus is apparent when we compare the values to the critical cluster size of $\simeq$32 Å estimated by Larson and Garside[53] using classical nucleation theory. The classical nucleation theory clearly overestimates the size of the critical nucleus for the $CO_2$ hydrate system. We now describe the nucleation process by a

path in the multidimensional order parameter space, and calculate the free energy associated with the path using the Landau–Ginzburg formalism.

### C. Labile cluster hypothesis

Sloan[4] proposed ''the labile cluster hypothesis'' as a viable pathway for nucleation, according to which ''labile clusters'' (a labile cluster being one $CO_2$ molecule encaged by 20–24 water molecules in its first coordination shell) diffuse in the liquid phase as a single entity. The critical nucleus is formed by the agglomeration of the labile clusters. Although this hypothesis was proposed more than a decade ago, there have been no theoretical or experimental attempts to validate the proposed mechanism. A previous computer simulation study showed evidence of the presence of labile clusters only for very dilute concentrations of the hydrophobic solute.[34] In order to test the labile cluster hypothesis, we define two classes of order parameters: the first being the coordination number of a randomly chosen $CO_2$ molecule, defined as the number of $H_2O$ molecules that are less than a distance $r_{nn}^{gh}$ where $r_{nn}^{gh}$ is defined based on $g_{gh}(r)$, similar to the cutoff, $r_{nn}^{hh}$, defined earlier. A labile cluster is identified as a $CO_2$ molecule along with the water molecules in its first coordination shell, if the coordination number is greater than or equal to twenty. The second class of order parameters are chosen to be the distance between labile clusters, defined as the carbon–carbon distance between the two $CO_2$ molecules that are part of the labile clusters. If the labile cluster hypothesis were to provide the correct nucleation mechanism, then

(a) the formation of the labile cluster would have to be either spontaneous, or an activated process *and* the labile cluster would exist as a metastable state (defined as a local minimum in the Landau free energy hypersurface);
(b) agglomeration of labile clusters would have to be spontaneous, *or* an activated process with an activation energy less than that of the free energy barrier for the disintegration of the metastable labile cluster.

We calculated the Landau free energy surface as a function of the order parameters associated with the labile cluster hypothesis, by using the Landau free energy method outlined in Sec. II. The first-order distribution functions of the free energy hypersurface in Figs. 4 and 5(a) clearly show evidence that is contrary to the above-mentioned criteria. In Fig. 4 is shown the free energy of formation of a labile cluster for three different concentrations of $CO_2$. $X_{CO_2}=0.011$: the saturation concentration of $CO_2$ in water, $X_{CO_2}=0.11$: the concentration of $CO_2$ that is equal to that in the clathrate hydrate with only the large cages occupied, $X_{CO_2}=0.14$: the concentration of $CO_2$ that is equal to that in the clathrate hydrate with complete occupancy. The activation free energy for the formation of the labile cluster is $3k_BT$ for $X_{CO_2}=0.011$, $10k_BT$ for $X_{CO_2}=0.11$, and $18k_BT$ for $X_{CO_2}=0.14$. Therefore, to describe step 1 of the labile cluster hypothesis, the labile clusters are easily formed by an activated process only for the case of dilute solutions. For concentrations near the $CO_2-H_2O$ interface, the free energy penalty for the formation of the labile clusters is large. In Fig. 5(a), we have depicted the results for the agglomeration of labile clusters, step 2 of the labile cluster hypothesis. The order parameters we have used to describe this process are given in Fig. 5(b), where, each hexagon filled with the pattern represents a labile cluster. For example, the distance between an agglomerate of four labile clusters and an isolated labile cluster is denoted by L(1,2,3,4)–L(5). Two labile clusters merge into a larger cluster when the distance between them reduces to about 6 Å. From Fig. 5(a), it is evident that the free energy barrier that has to be overcome for the agglomeration of two labile clusters is of the order of $35k_BT$, which is much larger than the stabilization free energy of the labile cluster (which is of the order of $1k_BT$, see Fig. 4). Therefore, it is thermodynamically favorable for the labile clusters to disintegrate rather than agglomerate to form a larger cluster. The free energy barrier that has to be overcome for forming larger clusters is too large and increases with increase in cluster size [Fig. 5(a)]. Thus, the violation of the above-mentioned two criteria are more pronounced as the size of the agglomerate increases and as the concentration of $CO_2$ in water increases. To build the critical nucleus (of size 14.5 Å), 32 labile clusters need to agglomerate, therefore, the free energy of formation of the critical nucleus according to the labile cluster hypothesis would be much greater than $150k_BT$, leading to a rate of formation that is less by several orders of magnitude than that observed in the experiments. Moreover, in our simulations, the agglomerated labile clusters do not undergo the necessary structural change to effect the nucleation of the clathrate phase. Therefore, we conclude that it is highly unlikely that the $CO_2$ hydrate nucleation occurs via the labile cluster hypothesis. In other words, the coordination number of a $CO_2$ molecule and the distance

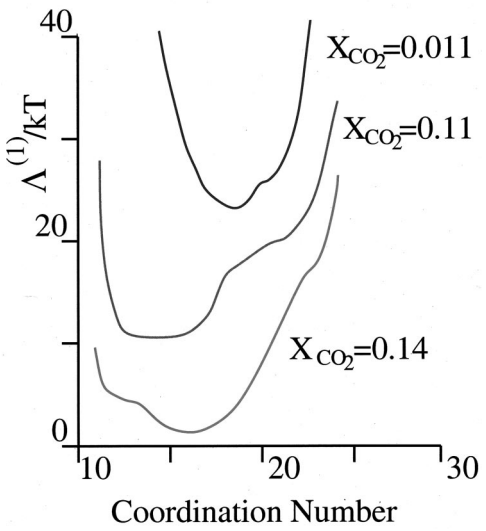


FIG. 4. Formation of a ''labile cluster:'' First-order distribution function of the Landau free energy, $\Lambda^{(1)}$ [coordination number] vs the coordination number of $H_2O$ molecules around a $CO_2$ molecule at three different concentrations. The free energy functions clearly indicate that the labile cluster is not a metastable state.

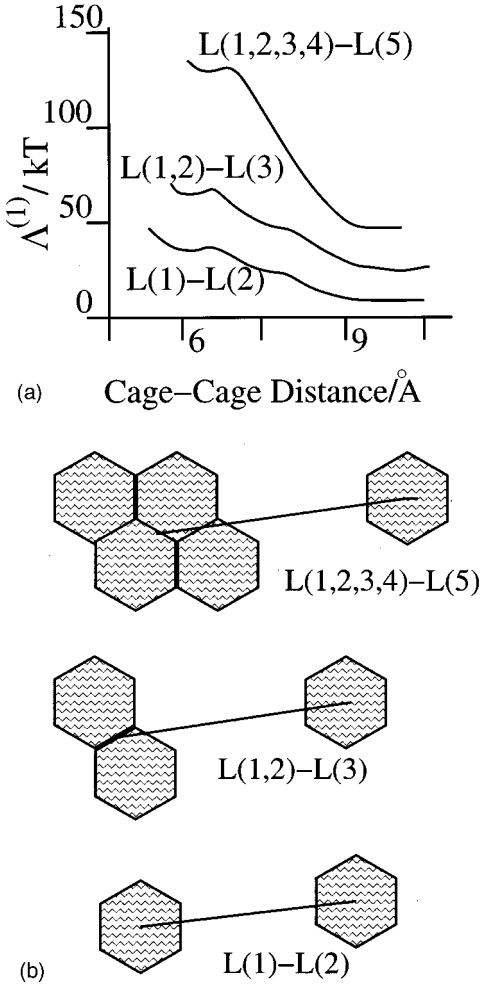


FIG. 5. Agglomeration of ''labile clusters:'' (a) First-order distribution function of the Landau free energy, $\Lambda^{(1)}[L]$, vs distance between labile clusters for three different sizes of agglomerates, at a mole fraction of $X_{CO_2}=0.14$. The distance between the labile clusters are defined pictorially in (b).

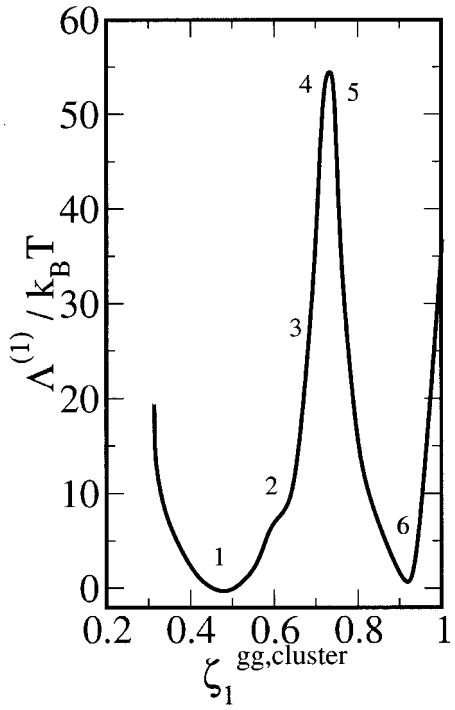


FIG. 6. The first-order distribution function of the Landau free energy hypersurface, $\Lambda^{(1)}[\zeta_1^{gg,cluster}]$ for a cluster of size 14.5 Å, showing the transformation from a liquid-like cluster to a clathrate-like cluster, eventually leading to the nucleation of the clathrate phase.

between labile clusters are not the correct set of order parameters to describe the nucleation of the clathrate hydrate.

### D. Local structuring hypothesis

As observed in Fig. 3, the first-order distribution function $\Lambda^{(1)}[W_4^{gg,cluster}]$ for the 9.6 Å shows an inflection at a value of $W_4^{gg,cluster}=0.133$, the value corresponding to the clathrate phase (see Table I), while that for the 14.5 and 19.3 Å clusters show a global minimum at $W_4^{gg,cluster}=0.15$. Therefore, evidence from cluster-implant studies (Fig. 3) indicates that the dissolution of implanted clusters smaller than the critical cluster size is initiated by the disappearance of order along the $W_4^{gg}$ coordinate. The free energy hypersurface along the $\zeta_1^{gg,cluster}$ coordinate is stable for clusters larger than the critical cluster size and metastable for clusters smaller than the critical cluster size. The free energy hypersurface along the host–host order parameter, $\zeta^{hh,cluster}$, is stable around the values in the clathrate phase ($\zeta^{hh,cluster}=1.0$) for the clusters larger than the critical nucleus, however displays a broad minimum ranging from $0.6<\zeta_1^{gg,cluster}<0.85$. For a 9.6 Å cluster, the number of water molecules in the cluster is comparable to that in the interface between the cluster and the liquid. Since the water molecules in this interface are also counted in determining the cluster order parameter $\zeta^{hh,cluster}$ [see Eq. (12)], the value of $\zeta^{hh,cluster}$ is less than that of the clathrate phase. A viewing of the snapshots during the simulation showed that the water molecules were structured (similar to those in the clathrate phase) even for small clusters, as long as the order along the $W_4^{gg,cluster}$ remained.

In light of the above-mentioned sets of observations, we propose ''the local structuring hypothesis'' to describe the mechanism of nucleation. The set of events described in the following initiate the nucleation of the clathrate phase.

(1) A thermal fluctuation causes a group of the guest ($CO_2$) molecules to be arranged in a configuration similar to that in the clathrate phase. The structure of the water molecules around the locally ordered guest molecules is also perturbed, in comparison with the bulk mixture. This process is to be regarded as a thermodynamic perturbation of the isotropic liquid phase due to the finite temperature of the system and hence, is stochastic in nature.

(2) If the number of guest molecules in the local ordered arrangement exceeds that in a critical nucleus, the relaxation of the surrounding water and $CO_2$ molecules causes the free energy hypersurface to be locally stable along all the guest–guest cluster order parameter coordinates. The guest–guest and the host–host cluster order parameters take on values close to the clathrate phase, resulting in the formation of the critical nucleus.

Thus, according to the local structuring hypothesis, a local geometrical arrangement of $CO_2$ molecules (whose symmetry is similar to that existing in the clathrate) caused

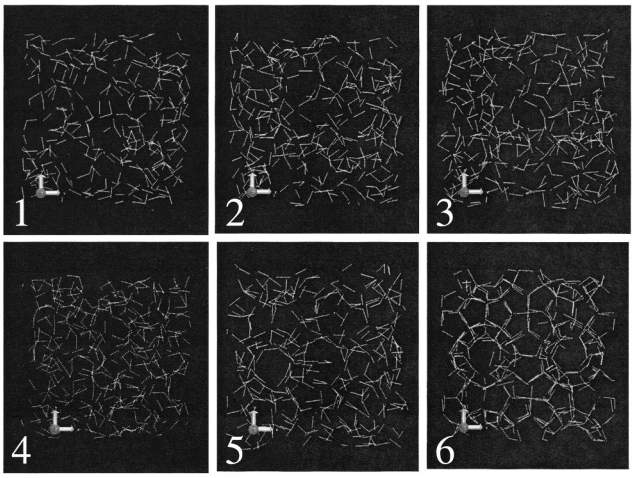


FIG. 7. Snapshots of the molecular configurations are shown in the form of distribution of hydrogen bonds in space. The cubical subvolume of the whole system encompassing the cluster is shown. Six different snapshots along the path of nucleation are depicted. The numbers correspond to the numbers marked along the free energy surface in Fig. 6 (see Table II for the evolution of the cluster order parameters along the path of nucleation).

by thermal fluctuations, leads to the formation of the critical nucleus.

An extreme case of the local structuring hypothesis was investigated by Hirai and co-workers.[54] The authors performed molecular dynamics simulations on water–$CO_2$ mixtures in which the positions of the $CO_2$ molecules were held fixed at the exact positions found from the crystal structure of the clathrate phase. The molecular dynamics was then performed only on the water molecules. The authors showed that starting from a disordered water phase, the water molecules organized themselves into a clathrate arrangement during the course of the molecular dynamics simulation.

Nucleation of clathrates can be described by a path in the four-dimensional order-parameter space ($W_4^{\mathrm{gg}}, \zeta_1^{\mathrm{gg}}, \zeta_2^{\mathrm{gg}}, \zeta^{\mathrm{hh}}$) that connects the liquid phase to the clathrate phase. Note that a path in order-parameter space is obtained by the ensemble average of several million configurations [see Eq. (9)]; therefore what we call a path, is a volume element in order-parameter space rather than a line. In order to describe the clathrate nucleation process, we assumed that the critical cluster size is equal to 14.5 Å and used a large system size (48 Å cubic box) to ensure minimal effects due to finite system size. We started with a well equilibrated liquid phase at mole fraction, $X_{\mathrm{CO_2}}=0.14$ and performed umbrella sampling in the four-dimensional cluster order-parameter space ($W_4^{\mathrm{gg,cluster}}, \zeta_1^{\mathrm{gg,cluster}}, \zeta_2^{\mathrm{gg,cluster}}, \zeta^{\mathrm{hh,cluster}}$) as outlined in Sec. II. The principal order parameter ($\Phi_1$ in Sec. II) was chosen to be $\zeta_1^{\mathrm{gg,cluster}}$, because onset of order along this coordinate is a pre-requisite for guest–guest ordering. Furthermore, it is clear that in increasing the value of $\zeta_1^{\mathrm{gg,cluster}}$, the system has to do work against the hydrophobic effect. Therefore, it is reasonable to expect that the least probable of the thermodynamic fluctuations is one that favors ordering along the $\zeta_1^{\mathrm{gg,cluster}}$ coordinate. The other three order-parameter coordinates were left to evolve freely as the system explored the phase space during the $NPT$ simulations. The first-order distribution function of the Landau free energy hypersurface with respect to the coordinate $\zeta_1^{\mathrm{gg,cluster}}$ is shown in Fig. 6. Starting from the liquid phase, six different snapshots along the path of nucleation are shown in Fig. 7, corresponding to points 1–6 in Fig. 6; the corresponding free energy changes along the path are summarized in Table II. We reiterate that the term ''path'' is indeed a volume element in order-parameter space and not a line. To bring about this fact clearly and give an idea of the size of the volume element, we provide in Table II the bounds of the distributions of the three order parameters ($W_4^{\mathrm{gg,cluster}}, \zeta_2^{\mathrm{gg,cluster}}, \zeta^{\mathrm{hh,cluster}}$) at various points along the path. In each volume element on the path, the bounds are reported as the minimum and the maximum values of the order parameters corresponding to the configurations that the system had visited. The snapshots clearly show the transformation from the liquid like cluster to a cluster resembling the clathrate, leading us to conclude that the chosen four order parameters are sufficient to describe nucleation of the clathrate phase.

TABLE II. Free energy change along the path of nucleation.

| Index | $\zeta_1^{\mathrm{gg,cluster}}$ | $\zeta_2^{\mathrm{gg,cluster}}$ | $\zeta^{\mathrm{hh,cluster}}$ | $W_4^{\mathrm{gg,cluster}}$ | $G/k_BT$ |
|---|---|---|---|---|---|
| 1 | 0.43 | 0.67 | 0.63 | −0.07–0.05 | 0 |
| 2 | 0.70 | 0.68–0.72 | 0.73 | −0.07–0.08 | 11 |
| 3 | 0.78 | 0.75–0.78 | 0.75 | 0.0–0.12 | 31 |
| 4 | 0.80 | 0.78–0.80 | 0.76 | 0.03–0.15 | 54 |
| 5 | 0.84 | 0.81 | 0.80 | 0.03–0.15 | 48 |
| 6 | 0.92 | 0.82–0.88 | 0.88 | 0.09–0.15 | −3 |

Convincing evidence to support the local structuring hypothesis is provided in Fig. 8, in which slices of the Landau free energy hypersurface, $\Lambda^{\mathrm{slice}}[W_4^{\mathrm{gg,cluster}}]$, along the $W_4^{\mathrm{gg,cluster}}$ coordinate, at six different regions along the path of nucleation, are shown for the 14.5 Å cluster. A slice of the Landau free energy hypersurface along an order-parameter coordinate is calculated by collecting a histogram of the one-dimensional probability function with respect to the order parameter as the system traverses the nucleation path. For the $\Lambda^{\mathrm{slice}}[W_4^{\mathrm{gg,cluster}}]$ functions marked 1,2, and 3, the global minimum corresponds to a liquid-like configuration within the 16 Å cluster. Note that points 1, 2, and 3 also have liquid-like values for the order parameters $\zeta^{\mathrm{hh,cluster}}$ and $\zeta_1^{\mathrm{gg,cluster}}$. The guest–guest ordering ($\zeta_1^{\mathrm{gg,cluster}}$) sets in be-

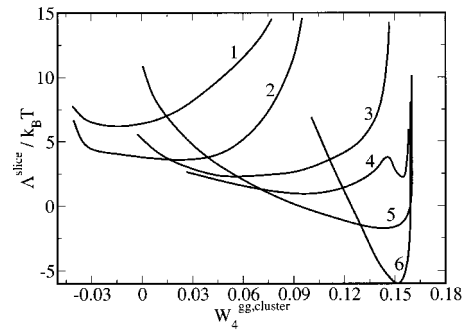


FIG. 8. The slices of the Landau free energy hypersurface, $\Lambda^{\mathrm{slice}}[W_4^{\mathrm{gg,cluster}}]$, at six different regions (marked in Fig. 6) are shown (a slice of the Landau free energy surface is different from, and not to be confused with, the first-order distribution function, which is a projection of the free energy surface along that coordinate). As earlier, numbers correspond to the numbers marked along the free energy surface in Fig. 6.

tween points 2 and 5 along the path. At point 4, there is a significant change in the function, $\Lambda^{\text{slice}}[W_4^{\text{gg,cluster}}]$, which now displays a metastability near $W_4^{\text{gg,cluster}}=0.13$, although the global minimum is still at liquid-like values of $W_4^{\text{gg,cluster}}$. The water molecules spontaneously relax between points 4 and 6 along the path, simultaneously, $\Lambda^{\text{slice}}[W_4^{\text{gg,cluster}}]$ changes shape to possess a global minimum at clathrate-like values in the cluster ($W_4^{\text{gg,cluster}}=0.14$). Point 5 along the path marks the end of the relaxation of the water molecules to the local–guest perturbation, at which point the cluster resembles a clathrate structure (see snapshot 5 in Fig. 7). The path from point 5 to point 6 marks the commencement of the growth of the clathrate phase from the cluster, as described in the section on cluster implants. The above-mentioned set of observations are exactly in accordance with the postulated local structuring hypothesis.

The free energy penalty, $\Delta F_{\text{path}}$, associated with the path of nucleation is defined by the free energy barrier along the path [the free energy barrier is the difference in free energy between the liquid phase and the saddle point on the path that has the largest (positive) free energy ($\Delta F_{\text{path}}=G_{\text{liquid}}-G_{\text{saddle}}$)] is calculated using 11. The saddle point for the Landau free energy hypersurface occurs between points 4 and 5 along the nucleation path, (see Fig. 6). The snapshot 5 in Fig. 7, verifies that the saddle indeed coincides with the formation of the critical nucleus. Therefore the reversible work for embryo formation is exactly equal to $\Delta F_{\text{path}}$. The free energy barrier associated with the nucleation calculated using Eq. (11) is equal to $55k_BT$.

In order to calculate the rate of nucleation from the nucleation barrier we used transition state theory (TST).[55] In using TST, the system is assumed to be in local thermodynamic equilibrium during the process of nucleation. The nucleation rate is calculated using

$$k=\frac{k_BT}{h}\exp\left(-\frac{\Delta F}{k_BT}\right), \tag{13}$$

where $\Delta F$ is the free energy barrier for nucleation, and the ratio $(k_BT)/h$ is the *frequency factor*, equal to $4.68\times10^{12}\,\text{s}^{-1}$ at 220 K. The rate of nucleation in the simulation cell [volume $V=(48\,\text{Å})^3$] is calculated to be $6.08\times10^{-12}\,\text{s}^{-1}$. For the case of homogeneous nucleation, the rate of nucleation is proportional to volume,[56] therefore in a macroscopic volume $V$, the rate of nucleation is given by $k=6.08\times10^{-12}V/V_{\text{critical nucleus}}$.

## IV. DISCUSSION AND CONCLUSIONS

Based on the Landau–Ginzburg free energy calculations, the critical cluster size for the nucleation of $CO_2$ clathrate hydrate at the liquid–liquid interface of $CO_2$ and $H_2O$ at 220 K and 4 MPA was calculated to be between 9.6 and 14.5 Å. This is to be compared with the result of classical nucleation theory, which predicts a critical size of 32 Å. It was shown that the mechanism of hydrate nucleation is in accord with the ''local structuring hypothesis.'' A quantitative estimation of the free energy barrier to nucleation was obtained using a path integral method, which samples the four-dimensional order-parameter space. The precise free energy difference between the liquid phase and the transition state, and the transition state and the hydrate phase was calculated. Teng *et al.*[21,22] and Mori *et al.*[10,11] have reported that the time scale for the nucleation of the $CO_2$ clathrate hydrate in their experiments to be of the order of 1–5 s. These experiments typically employed a $CO_2$ droplet of diameter, $D=1$ mm. Assuming that the interface, $\delta$, is 10 Å wide (see section III A on $CO_2-H_2O$ interface), the volume accessible for nucleation in the experiments is $V=0.25\times\pi\times D^2\delta$, equal to $7.8\times10^{14}\,(\text{Å})^3$. The time constant, $\lambda=1/k$, predicted by our simulation results for the experimental volume is 1.2 s. The significance of $\lambda$ is that, if we start out with $N$ identical samples at $t=0$, then after the passage of time $t=\lambda$, two-thirds of the samples will undergo nucleation.[57] Therefore our prediction agrees reasonably well with the experimental observations. In order to provide error bars on the computed rate of nucleation, it must be recognized that the rate scales linearly with the error involved in calculating the accessible volume for nucleation, whereas it scales exponentially with the error involved in calculating the $\Delta F$. The former can lead to a change in rate by a factor of $\delta/(V^{1/3}_{\text{critical nucleus}})\approx3$, while the latter leads to a change in rate by a factor of $\exp(2)\approx10$ because the intrinsic error in computing $\Delta F$ is of the order of $2k_BT$. However, the effect of the concentration of $CO_2$ on $\Delta F$ is not trivial to speculate and should be undertaken in a separate study.

We conclude by stating the main assumptions in our free energy approach. (1) Finite system size of our simulations do not alter the free energy barrier to nucleation. Free energy barriers are known to be strongly dependent on system size. However, for the state conditions we have chosen, the volume of the simulation cell is thirty times the volume of the critical cluster. Therefore it is our opinion that the calculated free energy barrier will be close to the infinite system. However, a system size scaling analysis[58] is necessary to validate this assumption, which is currently beyond our computational capabilities. (2) Nucleation is governed by equilibrium thermodynamics. This carries with it the assumptions made in the transition state theory. (3) The set of order parameters that we have chosen is complete, i.e., the minimum free energy path to nucleation lies within our chosen order parameter space.

A more rigorous approach that is devoid of assumptions 2 and 3 is based on ''transition path sampling'' described by Chandler *et al.*[59–61] We are currently implementing this based on the initial pathway found in the current study.

Ongoing work in our group involves investigation of a mechanism for the homogeneous nucleation of ice from liquid water and nucleation of natural gas hydrates at the vapor liquid interface of water and natural gas.

## ACKNOWLEDGMENTS

We are thankful to Howard Herzog for numerous helpful discussions on nucleation of $CO_2$ clathrates and ocean carbon sequestration. We acknowledge funding from the DOE Office of Science and the DOE Center for Research on Ocean Carbon Sequestration (DOCS).

[1] H. Herzog, E. Drake, and E. Adams, White Paper Final Report, DOE Order No. DE-AF22-96PCO1257, 1997.
[2] H. Herzog, K. Caldeira, and E. Adams, *Carbon Sequestration via Direct Injection*, Encyclopedia of Ocean Sciences Vol. 1, edited by J. Steele, S. Thorpe, and K. Turekian (Academic, London, 2001), 408 pp.
[3] H. Herzog, B. Eliasson, and O. Kaarstad, Sci. Am. **281**, 53 (2000).
[4] D. Sloan, *Clathrate Hydrates of Natural Gases* (Marcel Dekker, New York, 1998).
[5] A. Demurov, R. Radhakrishnan, and B. L. Trout, J. Chem. Phys. **116**, 702 (2002).
[6] R. Radhakrishnan, A. Demurov, H. Herzog, and B. L. Trout, Energy Convers. Manage. (to be published).
[7] W. S. Dodds, L. F. Stutzman, and B. J. Sollami, Ind. Eng. Chem., Chem. Eng. Data Series **1**, 92 (1956).
[8] K. Y. Song and R. Kobayashi, SPE Form. Eval. **2**, 501 (1987).
[9] M. Wendland, H. Hasse, and G. Maurer, J. Chem. Eng. Data **44**, 901 (1999).
[10] R. Ohmura and Y. H. Mori, J. Chem. Eng. Data **44**, 1432 (1999).
[11] Y. H. Mori and T. Mochizuki, Energy Convers. Manage. **39**, 567 (1998).
[12] I. Aya, K. Yamane, and N. Yamada, Proceedings of the Winter Annual Meeting of ASME, HTD, Vol. 215, 1992, p. 17.
[13] Y. Fujioka, K. Takeuchi, Y. Shindo, and H. Komiyama, Int. J. Energy Res. **18**, 765 (1994).
[14] I. Aya, K. Yamane, and N. Yamada, Proceedings of the International Symposium on $CO_2$ Fixation and Efficient Utilization of Energy, 1993, p. 351.
[15] A. Saji, H. Noda, Y. Takamura, T. Takata, H. Kitamura, and T. Kamata, Energy Convers. Manage. **36**, 493 (1995).
[16] H. Kimuro, F. Yamaguchi, K. Ohstubo, T. Kusayanagi, and M. Morishita, Energy Convers. Manage. **34**, 1089 (1993).
[17] H. Kimuro, T. Kusayanagi, F. Yamaguchi, K. Ohtsubo, and M. Morishita, IEEE T. Energy Conver. **9**, 732 (1994).
[18] S. Hirai, K. Okazaki, N. Araki, K. Yoshimoto, H. Ito, and K. Hijikata, Energy Convers. Manage. **36**, 471 (1995).
[19] H. Nishikawa, M. Ishibashi, H. Ohta, H. Akutsu, M. Tajika, T. Sugitani, R. Hiraoka, H. Kimuro, and T. Shiota, Energy Convers. Manage. **36**, 489 (1995).
[20] R. P. Warzinski, P. D. Bergman, S. P. Masutani, and G. D. Holder, Am. Chem. Soc., Div. Fuel. Chem. **42**, 578 (1997).
[21] H. Teng and A. Yamasaki, Int. J. Heat Mass Transf. **41**, 4315 (1998).
[22] K. Ogaswara, A. Yamasaki, and H. Teng, Energy Fuels **15**, 147 (2001).
[23] Y. H. Mori, Energy Convers. Manage. **39**, 1537 (1998).
[24] S. Hirai, K. Okazaki, N. Araki, H. Yazawa, H. Ito, and K. Hijikata, Energy Convers. Manage. **37**, 1073 (1996).
[25] M. Volmer and A. Weber, Z. Phys. Chem., Stoechiom. Verwandtschaftsl. **119**, 277 (1924).
[26] F. F. Abraham, *Homogeneous Nucleation Theory* (Academic, New York, 1974), Chap. 5.
[27] P. G. Debenedetti, *Metastable Liquids* (Princeton University Press, Princeton, 1996).
[28] P. R. Bishnoi, V. Natarajan, and N. Kalogerakis, Ann. N.Y. Acad. Sci. **912**, 311 (2000).
[29] P. N. Englezos, N. Kalogerakis, P. D. Dholabhai, and P. R. Bishnoi, Chem. Eng. Sci. **42**, 2659 (1987).
[30] P. D. Dholabhai, N. Kalogerakis, and P. R. Bishnoi, Can. J. Chem. Eng. **71**, 68 (1993).
[31] S. M. Thomson, K. E. Gubbins, J. R. P. B. Walton, R. R. Chantry, and J. S. Rowlinson, J. Chem. Phys. **81**, 530 (1984).
[32] R. L. Christiansen and E. D. Sloan, Ann. N.Y. Acad. Sci. **912**, 283 (2000).
[33] E. D. Sloan and F. Flayfel, AIChE J. **37**, 1281 (1991).
[34] S. Swaminathan, S. W. Harrison, and D. L. Beveridge, J. Am. Chem. Soc. **100**, 5705 (1978).
[35] B. Kvamme, Ann. N.Y. Acad. Sci. **912**, 306 (2000).
[36] W. L. Jorgensen, J. Chandrasekhar, and J. D. Madura, J. Chem. Phys. **79**, 926 (1993).
[37] J. G. Harris and K. H. Yung, J. Phys. Chem. **99**, 12021 (1995).
[38] J. R. Errington, K. Kiyohara, K. E. Gubbins, and A. Z. Panagiotopoulos, Fluid Phase Equilib. **150**, 33 (2000).
[39] O. A. Karim and A. D. J. Haymet, J. Chem. Phys. **89**, 6889 (1988).
[40] M. J. Vlot, J. Huinink, and J. P. van der Eerden, J. Chem. Phys. **110**, 55 (1999).
[41] G. T. Gao and X. C. Xeng, J. Chem. Phys. **112**, 8534 (2000).
[42] P. M. Chaikin and T. C. Lubinski, *Principles of Condensed Matter Physics* (Cambridge University Press, Cambridge, 1995).
[43] T. V. Ramakrishnan and M. Yussouff, Phys. Rev. B **19**, 2775 (1979).
[44] P. J. Steinhardt, D. R. Nelson, and M. Ronchetti, Phys. Rev. B **28**, 784 (1983).
[45] L. D. Landau and E. M. Lifshitz, *Quantum Mechanics* (Pergamon, New York, 1965).
[46] P. L. Chau and A. J. Hardwick, Mol. Phys. **93**, 511 (1998).
[47] J. R. Errington and P. G. Debenedetti, Nature (London) **409**, 318 (2001).
[48] R. Radhakrishnan and K. E. Gubbins, Mol. Phys. **96**, 1249 (1999).
[49] R. M. Lynden-Bell, J. S. Van Duijneveldt, and D. Frenkel, Mol. Phys. **80**, 801 (1993).
[50] L. D. Landau and E. M Lifshitz, *Statistical Physics*, 3rd ed. (Pergamon, London, 1980).
[51] G. M. Torrie and J. P. Valleau, Chem. Phys. Lett. **28**, 578 (1974).
[52] L. A. Báez and P. Clancy, Ann. N.Y. Acad. Sci. **715**, 177 (1994).
[53] M. A. Larson and J. Garside, Chem. Eng. Sci. **41**, 1285 (1986).
[54] S. Hirai, K. Okazaki, Y. Tabe, and K. Kawamura, Energy Convers. Manage. **38**, S301 (1997).
[55] J. I. Steinfeld, J. S. Francisco, and W. L. Hase, *Chemical Kinetics And Dynamics* (Prentice—Hall, Upper Saddle River, NJ, 1998).
[56] T. Koop, B. Luo, A. Tsias, and T. Peter, Science **406**, 611 (2000).
[57] T. W. Barlow and A. D. J. Haymet, Rev. Sci. Instrum. **66**, 2996 (1995).
[58] J. Lee and J. M. Kosterlitz, Phys. Rev. Lett. **65**, 137 (1990).
[59] C. Dellago, P. G. Bolhuis, F. S. Csajka, and D. Chandler, J. Chem. Phys. **108**, 1964 (1998).
[60] C. Dellago, P. G. Bolhuis, and D. Chandler, J. Chem. Phys. **108**, 9236 (1998).
[61] P. G. Bolhuis, C. Dellago, and D. Chandler, Faraday Discuss. **110**, 421 (1998).